Journal of Nuclear Materials 408 (2011) 236–245

Contents lists available at ScienceDirect

Journal of Nuclear Materials

journal homepage: www.elsevier.com/locate/jnucmat

X-ray absorption studies of chlorine valence and local environments in borosilicate waste glasses

David A. McKeown [a,*], Hao Gan [a], Ian L. Pegg [a], W.C. Stolte [b], I.N. Demchenko [b]

[a] Vitreous State Laboratory, The Catholic University of America, 620 Michigan Ave, N.E., Washington, D.C. 20064, USA
[b] Department of Chemistry, University of Nevada, Las Vegas, NV 89154-4033, USA

ARTICLE INFO

Article history:
Received 5 August 2010
Accepted 18 November 2010
Available online 26 November 2010

ABSTRACT

Chlorine (Cl) is a constituent of certain types of nuclear wastes and its presence can affect the physical and chemical properties of silicate melts and glasses developed for the immobilization of such wastes. Cl K-edge X-ray absorption spectra (XAS) were collected and analyzed to characterize the unknown Cl environments in borosilicate waste glass formulations, ranging in Cl-content from 0.23 to 0.94 wt.%. Both X-ray absorption near edge structure (XANES) and extended X-ray absorption fine structure (EXAFS) data for the glasses show trends dependent on calcium (Ca) content. Near-edge data for the Ca-rich glasses are most similar to the Cl XANES of $CaCl_2$, where Cl^- is coordinated to three Ca atoms, while the XANES for the Ca-poor glasses are more similar to the mineral davyne, where Cl is most commonly coordinated to two Ca in one site, as well as Cl and oxygen nearest-neighbors in other sites. With increasing Ca content in the glass, Cl XANES for the glasses approach that for $CaCl_2$, indicating more Ca nearest-neighbors around Cl. Reliable structural information obtained from the EXAFS data for the glasses is limited, however, to Cl—Cl, Cl—O, and Cl—Na distances; Cl—Ca contributions could not be fit to the glass data, due to the narrow *k*-space range available for analysis. Structural models that best fit the glass EXAFS data include Cl—Cl, Cl—O, and Cl—Na correlations, where Cl—O and Cl—Na distances decrease by approximately 0.16 Å as glass Ca content increases. XAS for the glasses indicates Cl^- is found in multiple sites where most Cl-sites have Ca neighbors, with oxygen, and possibly, Na second-nearest neighbors. EXAFS analyses suggest that Cl—Cl environments may also exist in the glasses in minor amounts. These results are generally consistent with earlier findings for silicate glasses, where Cl^- was associated with Ca^{2+} and Na^+ in network modifier sites.

1. Introduction

One of the standard treatment technologies for the immobilization of radioactive wastes, and high-level radioactive wastes in particular, is vitrification to form a borosilicate glass. Many such wastes contain chlorine (Cl) [1], which is generally sparingly soluble in borosilicate glasses. Furthermore, the presence of chlorine can affect the solubility of other sparingly soluble species, such as sulfates and chromates, and may ultimately limit the waste loading in the glass. Excessive levels of these constituents can lead to phase separation in the melt with the formation of deleterious corrosive molten salt phases. Glass formulation modifications that can result in increased solubility of these species can, in principle, be guided by a better understanding of their local chemical and structural environments within the borosilicate glass matrix. At present, in the case of Cl, such information is very limited. In addition to these issues, the role of Cl is also of interest with regard to effects it may have on the durability and leachability of borosilicate glasses used for long-term radioactive waste storage. Recent studies of Cl in amorphous silicates used X-ray absorption spectroscopy (XAS) and nuclear magnetic resonance (NMR) techniques to characterize Cl in alkali and alkaline earth aluminosilicate tetrahedral network materials [2–4]. In the present work, XAS is used to characterize the average Cl valence and nearest-neighbor environment in borosilicate glasses, which will be compared with these earlier findings for Cl in silicate glasses.

An X-ray absorption spectrum is divided into two regions: the X-ray absorption near edge structure (XANES) that includes an absorption edge of the element of interest (in this case, Cl); and the extended X-ray absorption fine structure (EXAFS). Typically, the edge energy is sensitive to the valence of the absorbing element, which increases with the higher valence of the absorber. Features at the absorption edge are also sensitive to the local atomic environment surrounding Cl. The EXAFS data, by convention, are extracted from a spectrum at approximately 20 eV beyond the absorption edge to higher energies. In many cases, EXAFS oscillations are due primarily to single scattering of the spherical electron wave emitted by the absorbing atom from the arrangement of surrounding atoms. Through fitting procedures, EXAFS data are

* Corresponding author. Tel.: +1 202 319 5226; fax: +1 202 319 4469.
E-mail address: davidm@vsl.cua.edu (D.A. McKeown).

0022-3115/$ - see front matter © 2010 Elsevier B.V. All rights reserved.
doi:10.1016/j.jnucmat.2010.11.035

Table 1
Major oxide compositions from XRF analyses (wt.%) of the glasses: from low to high CaO content. Uncertainties are less than or equal to 10% of the value listed.

Glass	Network modifiers	Network formers	Transition metals	SO_3	Cl	Total
GWV-G-133B	Li_2O 3.50[a] Na_2O 17.45 MgO 1.49 CaO 1.88 K_2O 4.67	Al_2O_3 5.63 B_2O_3 9.99[a] P_2O_5 2.73 SiO_2 39.28	Cr_2O_3 0.77 Fe_2O_3 4.80 MnO 0.01 NiO 0.03 TiO_2 1.44 V_2O_5 0.01 ZnO 3.13 ZrO_2 2.52	0.34	0.23	99.9
GWV-G-65A	Li_2O 3.50[a] Na_2O 17.84 MgO 1.47 CaO 1.93 K_2O 4.35	Al_2O_3 5.81 B_2O_3 9.99[a] P_2O_5 0.32 SiO_2 41.11	Cr_2O_3 0.24 Fe_2O_3 4.87 MnO 0.01 NiO 0.03 TiO_2 1.50 ZnO 3.37 ZrO_2 2.68	0.31	0.51	99.84
LAWA44	Na_2O 20.00 MgO 1.99 CaO 1.99 K_2O 0.47	Al_2O_3 6.20 B_2O_3 8.90[a] P_2O_5 0.22 SiO_2 44.56	Cr_2O_3 0.20 Fe_2O_3 6.98 MnO 0.02 NiO 0.04 TiO_2 2.00 ZnO 2.96 ZrO_2 3.00	0.38	0.57	100.48
WVT-G-140A	Na_2O 17.75 MgO 1.74 CaO 2.05 K_2O 0.55	Al_2O_3 6.46 B_2O_3 8.99[a] P_2O_5 1.43 SiO_2 46.55	Cr_2O_3 0.16 Fe_2O_3 6.75 MnO 0.02 NiO 0.01 Re_2O_7 0.39 TiO_2 2.14 ZnO 3.14 ZrO_2 3.55	0.21	0.23	100.98
P10-G-90E	Na_2O 20.58 MgO 1.70 CaO 2.27 K_2O 5.19	Al_2O_3 6.92 B_2O_3 9.70[a] P_2O_5 0.27 SiO_2 40.18	Cr_2O_3 0.36 Fe_2O_3 5.85 MnO 0.02 NiO 0.07 TiO_2 1.26 ZnO 2.73 ZrO_2 2.17	0.37	0.24	99.88
P10-G-129A	Na_2O 19.87 MgO 1.31 CaO 2.29 K_2O 5.39	Al_2O_3 6.49 B_2O_3 9.70[a] P_2O_5 0.19 SiO_2 40.62	Cr_2O_3 0.24 Fe_2O_3 5.37 MnO 0.02 NiO 0.04 TiO_2 1.49 V_2O_5 0.03 ZnO 3.29 ZrO_2 2.27	0.38	0.91	99.9
[+]P10-G-79F	Na_2O 19.95 MgO 1.86 CaO 2.32 K_2O 4.49	Al_2O_3 6.62 B_2O_3 9.70[a] P_2O_5 0.74 SiO_2 40.08	Cr_2O_3 0.34 Fe_2O_3 5.93 MnO 0.02 NiO 0.05 TiO_2 1.29 ZnO 2.88 ZrO_2 2.34	0.36	0.94	99.91
FWV-G-138A	Li_2O 3.50[a] Na_2O 19.87 MgO 1.43 CaO 2.39 K_2O 0.53	Al_2O_3 5.86 B_2O_3 9.99[a] P_2O_5 0.16 SiO_2 42.53	Cr_2O_3 0.78 Fe_2O_3 5.09 MnO 0.02 NiO 0.03 TiO_2 1.36 V_2O_5 0.01 ZnO 3.29 ZrO_2 2.68	0.36	0.21	100.09
O10-G-57D	Na_2O 22.33 MgO 1.34 CaO 2.48 K_2O 0.56	Al_2O_3 6.28 B_2O_3 9.70[a] P_2O_5 0.17 SiO_2 44.16	Cr_2O_3 0.26 Fe_2O_3 4.96 MnO 0.02 NiO 0.04 TiO_2 1.30 V_2O_5 0.01 ZnO 3.19 ZrO_2 2.48	0.39	0.24	99.91

(*continued on next page*)

Table 1 (*continued*)

Glass	Network modifiers	Network formers	Transition metals	SO_3	Cl	Total
FWV-G-108B	Li_2O 3.50[a] Na_2O 19.68 MgO 1.49 CaO 2.63 K_2O 0.56	Al_2O_3 5.81 B_2O_3 9.70[a] P_2O_5 0.17 SiO_2 42.22	Cr_2O_3 0.24 Fe_2O_3 5.24 MnO 0.02 NiO 0.03 TiO_2 1.33 V_2O_5 0.01 ZnO 3.21 ZrO_2 2.47	0.36	0.61	99.89
O10-G-51A	Na_2O 21.14 MgO 1.34 CaO 2.98 K_2O 0.56	Al_2O_3 6.33 B_2O_3 9.70[a] P_2O_5 0.17 SiO_2 44.18	Cr_2O_3 0.24 Fe_2O_3 4.91 MnO 0.02 NiO 0.04 TiO_2 1.34 V_2O_5 0.01 ZnO 3.19 ZrO_2 2.48	0.38	0.86	99.87
N10-G-91E	Li_2O 4.00[a] Na_2O 12.43 MgO 1.33 CaO 5.52 K_2O 0.63	Al_2O_3 5.77 B_2O_3 17.00[a] P_2O_5 0.15 SiO_2 41.10	Cr_2O_3 0.16 Fe_2O_3 4.41 MnO 0.02 NiO 0.03 TiO_2 1.35 ZnO 2.89 ZrO_2 2.29	0.54	0.26	99.88
[+]N10-G-85D	Li_2O 4.00[a] Na_2O 11.33 MgO 1.43 CaO 5.63 K_2O 0.58	Al_2O_3 5.80 B_2O_3 17.00[a] P_2O_5 0.15 SiO_2 42.20	Cr_2O_3 0.15 Fe_2O_3 4.18 MnO 0.02 NiO 0.04 TiO_2 1.34 V_2O_5 0.01 ZnO 2.78 ZrO_2 2.18	0.37	0.74	99.83
N10-G-37A	Li_2O 4.00[a] Na_2O 5.87 MgO 1.75 CaO 6.04 K_2O 0.52	Al_2O_3 5.73 B_2O_3 17.00[a] P_2O_5 0.16 SiO_2 47.67	Cr_2O_3 0.22 Fe_2O_3 3.46 MnO 0.02 NiO 0.20 TiO_2 1.26 V_2O_5 0.01 ZnO 2.99 ZrO_2 1.79	0.54	0.65	99.88
[+]FWV-G-34C	Li_2O 3.50[a] Na_2O 6.51 MgO 3.02 CaO 6.92 K_2O 0.60	Al_2O_3 6.64 B_2O_3 9.99[a] P_2O_5 0.18 SiO_2 47.83	Cr_2O_3 0.24 Fe_2O_3 5.59 MnO 0.04 NiO 0.05 TiO_2 1.49 V_2O_5 0.05 ZnO 3.38 ZrO_2 2.90	0.63	0.27	99.83

[a] Target composition.
[+] EXAFS analysis presented in Table 3.

analyzed here to quantitatively determine average bond distance (r (Å)), coordination number (n (atoms)), and disorder (Debye–Waller factor or σ^2 (Å^2)) of shells of atoms around Cl.

Nine crystalline standards were measured to model the possible Cl valences and environments that may be found in the borosilicate glasses investigated, that include $NaClO_4$, $KClO_4$, $NaClO_3$, $NaClO_2$, NaCl (halite), KCl (sylvite), $CaCl_2$, sodalite ($Na_4Si_3Al_3O_{12}Cl$), and davyne (ideal formula: $Na_4K_2Ca_2Si_6Al_6O_{24}(SO_4)Cl_2$). $NaClO_4$ and $KClO_4$ have ClO_4^- tetrahedra containing Cl—O distances at 1.57 and 1.46 Å [5,6], respectively, surrounded by alkali cations that are major elemental components in the glasses studied. $NaClO_3$ has ClO_3 pyramids [7], where Cl is at the apex of each pyramid with 1.46 Å Cl—O distances. Chlorine in $NaClO_2$ is part of a bent O—Cl—O molecular configuration, where Cl—O distances are 1.56 Å [8]. Halite and sylvite standards have Cl surrounded by six alkali cations, where Cl—Na is 2.82 Å and Cl—K is 3.14 Å [9], respectively. In $CaCl_2$, Cl has three Ca nearest-neighbors in a nearly flat, almost trigonal pyramid configuration with Cl at the apex, with one Cl—Ca distance at 2.70 Å and two at 2.76 Å [10]. Cl^- in sodalite is tetrahedrally coordinated by four Na atoms at a distance of 2.74 Å [11]. Davyne has Cl within at least two sites surrounded by a linked SiO_4 and AlO_4 tetrahedra framework [12], where in one site, Cl has two Ca nearest-neighbors with Cl—Ca distances near 2.68 Å, and in the other site, Cl is within framework channels as Cl—Cl chains [12].

XAS data were collected for 15 chlorine-containing borosilicate glasses. Fourteen glasses were synthesized in continuously-fed ceramic refractory-lined joule-heated melters [13,14]. One glass formulation investigated (LAWA44) was synthesized in Pt–Au crucibles. To improve signal-to-noise ratios in the XAS data, the glasses investigated have Cl concentrations (Table 1) that are somewhat higher than typical waste glasses.

In previous work, XANES and NMR were used to characterize the Cl environments in silicate glasses and fly ash materials [2–4]. Preliminary investigations of Cl in alkali and alkaline earth silicate glasses indicate that Cl can be bonded to Ca in Ca-bearing melts in a salt-like environment similar to that in $CaCl_2{\cdot}2H_2O$ [2]. ^{35}Cl NMR studies of Cl-containing (Na, Ca) aluminosilicate glasses [3] indicate Cl^- environments surrounded by Ca^{2+} and Na^+ with

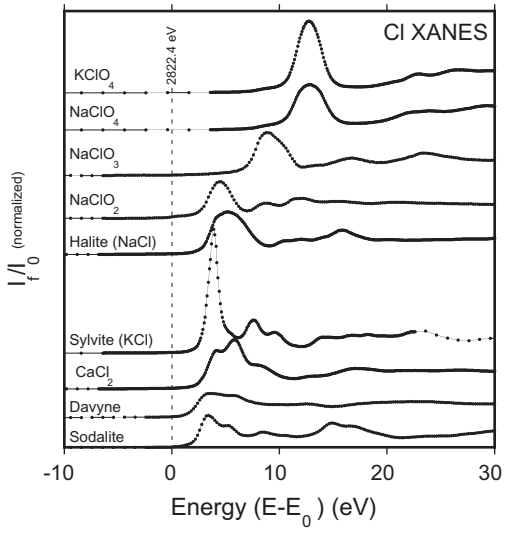

Fig. 1. Edge-step normalized XANES spectra of the chlorine standards, where E_0 is indicated. Plots are offset for clarity.

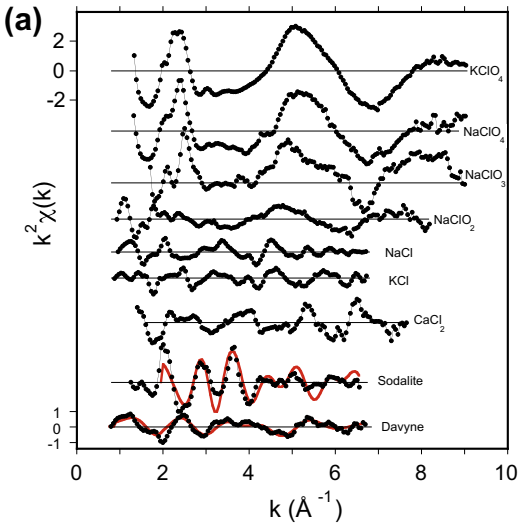

Fig. 3a. $k^2\chi(k)$ data for the Cl standards (points and line). Final fits from FEFFIT (red lines) for sodalite and davyne are plotted. Plots offset for clarity. (For interpretation of the references to colour in this figure legend, the reader is referred to the web version of this article.)

no evidence of Cl^- bonding directly to Al or Si. In the amorphous portions of silica-poor Ca- and Cl-rich fly ash materials, Cl can be in environments similar to those in NaCl, KCl, $CaCl_2$ and Friedel's salt ($Ca_2Al(OH)_6(Cl, OH)\cdot H_2O$) [4].

2. Experimental

The $NaClO_4$, $NaClO_3$, $NaClO_2$, $CaCl_2$, and $KClO_4$ samples were crystalline reagent powders obtained from Sigma–Aldrich. The halite (NMNH 103582), sylvite (NMNH 40223), sodalite (NMNH C4979, from Bolivia), and davyne (NMNH 141468, from Italy) samples were obtained from the Mineral Sciences Department, Smithsonian Institution. Phase identification was verified for each standard using X-ray diffraction (XRD) techniques. The sodalite sample contains minor amounts of K and Fe [15], while the davyne sample may contain minor amounts of sodalite and quadridavyne ($(Na, K)_6Cl_2)(Ca_2Cl_2)(Si_6Al_6O_{24})$) [16] according to XRD analysis. Quadridavyne has the davyne structure except that long-range ordering of (Na, K)- and Cl-sites within open channels doubles the a_0 unit cell parameter [16]; these structural differences lead to five different Cl-sites, where two of the sites are one sixth occupied by Cl. In quadridavyne, Cl can bond with itself to have Cl—Cl distances as small as 0.98 Å or as long as 3.42 Å. All standards were ground to powders and sieved to particle sizes $\leqslant$10 μm in diameter due to the soft X-ray energies used at the Cl K-absorption edge (near 2822 eV). One layer of particles was deposited on kapton tape. The $CaCl_2$, halite, and sylvite crystalline standards have high Cl concentrations and correspondingly small absorption lengths (<5 μm) at these energies, so that self-absorption corrections to the fluorescence XANES and EXAFS data were done using the programs FLUO [17] and SABCOR [18], respectively.

The glasses investigated were synthesized from reagent grade chemicals in crucibles or in DM10 or DM100 joule-heated melters [13,14] that hold approximately 8 and 110 kg of melt, respectively. The feed material for these melters is introduced as an aqueous slurry directly onto the surface of the molten borosilicate pool in the melter. The energy required to melt the feed is dissipated by

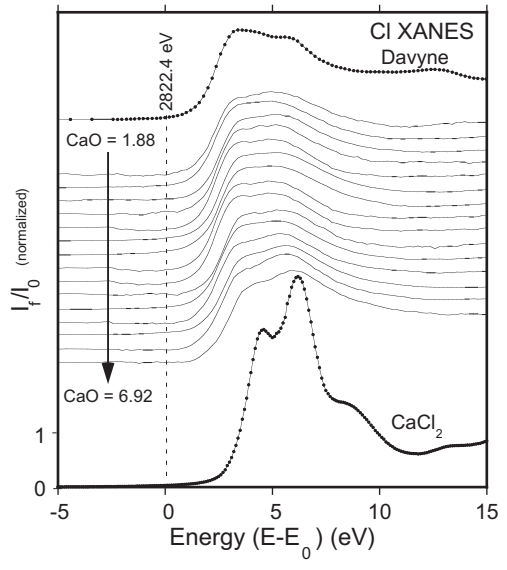

Fig. 2. Edge-step normalized XANES spectra of the standards davyne and $CaCl_2$ (points and line), as well as the glasses investigated (line only). The glasses are ordered from lowest (top line plot) to highest (bottom line plot) CaO-content indicated in wt.%. Conventions in Fig. 1 apply.

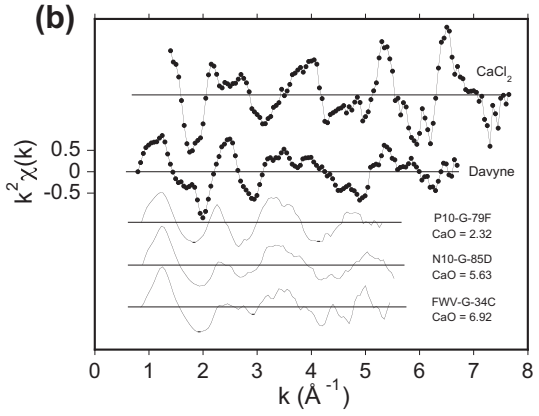

Fig. 3b. $k^2\chi(k)$ data for the $CaCl_2$ and davyne standards (points and line), as well as for three representative borosilicate glasses investigated (line), arranged from low (P10-G-79F) to high (FWV-G-34C) CaO content (in wt.%).

resistance heating that passes an electric current between plate electrodes through the molten glass pool. A bubbler is used in these melters to stir the melt. Due to the relatively low Cl concentrations (<1.0 wt.%) in the glasses, no self-absorption effects are expected, even for an infinitely thick sample. As a result, glass fragments were used for the XAS measurements to obtain the best signal-to-noise spectra and were taken from homogeneous portions of the glass sample. Chemical analyses of the glasses (Table 1) were performed by X-ray fluorescence (XRF) techniques.

Chlorine K-edge fluorescence XAS data were collected at the Advanced Light Source (ALS), Lawrence Berkeley National Laboratory (LBNL), on beamline 9.3.1 at a vacuum chamber pressure of 2×10^{-7} torr. For each spectrum collected, the double crystal Si (1 1 1) monochromator was scanned from 2760 to 3000 eV, where the scan parameters were 0.1 eV point spacing at 2 s per data point from approximately 10 eV below to 30 eV above the Cl K-edge, and 1 eV point spacing at 2 s per point for energies greater than 30 eV above the edge. Incident X-ray intensity (I_0) was measured using an Al-coated mylar foil, which was placed in the photon beam upstream of the sample. The current measured from the foil was monitored by a FEMTO Messtechnik BmbH (model DDPCA-300) subfemto-ampere current amplifier. Fluorescence X-ray intensities (I_f) from the sample were measured by a Hamamatsu (type S3584, 28 mm by 28 mm active area) Si photodiode connected to a Stanford Research Systems (model SR570) current amplifier. The analog outputs of both electrometers were fed directly into the data acquisition computer. The absorption coefficient (μ) of the sample at a particular energy is proportional to I_f/I_0. The X-ray absorption spectrum is a plot of μ versus energy in eV. The spectra were initially energy-calibrated to the $11a_1$ transition of CF_3Cl at 2823.5 eV [19]. Energy uncertainty for the data presented here is within ±0.2 eV, whereas the resolution is approximately 0.45 eV [20]. During the data collection, sodalite Cl XANES was collected periodically to correct for any monochromator energy drift over time. A minimum of three X-ray absorption spectra were collected for each sample.

3. Data analysis

The XANES spectra that are presented are averages of at least two data sets from each sample that were initially processed using standard pre-edge background subtraction and edge-step normalization procedures [21]. The energy at the base of the Cl K-absorption edge for sodalite was calibrated to 1.1 eV from the CF_3Cl transition (or at 2822.4 eV), defined to be E_0, and reset to 0 eV (Figs. 1 and 2). The K-absorption edge inflection point in each sodalite calibration spectrum was set to 2825 eV, to energy-calibrate the Cl K-absorption edge in each XANES spectrum for all other samples. After normalization and calibration, direct comparisons can be made with XANES data for all samples measured to an energy accuracy of ±0.2 eV, or the energy difference between two adjacent data points at the edge (Figs. 1 and 2).

Four EXAFS spectra were collected for most samples, where two data sets were averaged together. More spectra were collected and then averaged for the lower concentration Cl glasses, such as FWV-G-138A glass (0.21 wt.% Cl), where 15 spectra were collected. For each spectrum, a pre-edge linear background was subtracted, and the edge-step was normalized to unity. A cubic spline function was fit to and then subtracted from all edge-step normalized data at approximately 2.5–130 eV above E_0. Energy values in eV were converted to k (Å^{-1}) [21], where the resulting $\chi(k)$ data was k^2-weighted (Figs. 3a and 3b). EXAFS data for the Cl—silicate standards sodalite and davyne have narrow k-ranges ($0.9 \leqslant k \leqslant 6.6$ Å^{-1}) that contain discernable EXAFS oscillations. Due to larger structural disorder in amorphous structures, the resulting glass EXAFS k-ranges were even narrower, $0.9 \leqslant k \leqslant 5.5$ Å^{-1} (Figs. 3b and 4). A Hanning window of 0.5 Å^{-1} was used on the upper and lower limits of the data to minimize Fourier-transform termination artifacts in the resulting partial radial distribution function (RDF).

The chemical similarities of the two Cl—silicate standards to the glasses prompted full EXAFS analyses of the data for these two standards. The analyses for these standards provided guidelines to analyze the EXAFS data for three representative glasses, P10-G-79F, N10-G-85D, and FWV-G-34C which span the range of the trends in the EXAFS data as well as most of the CaO concentrations in the glasses (Figs. 3b, 4, 5b, and Table 1). Peaks in the RDFs correspond to shells of atoms surrounding Cl (Figs. 5a and 5b), where r, n, and σ^2 for each atomic shell can be obtained from the fitting

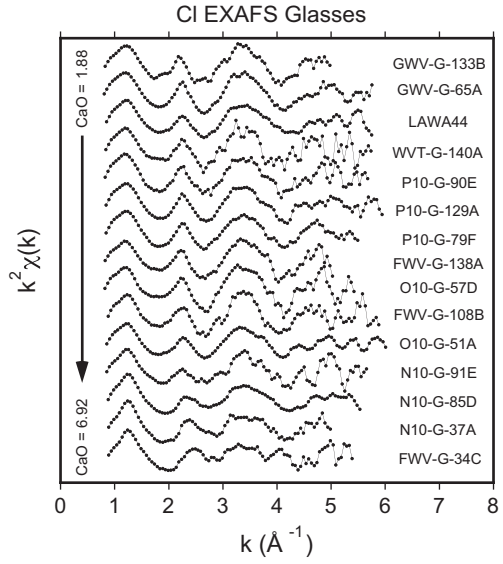

Fig. 4. $k^2\chi(k)$ data for the glasses investigated in order of CaO content (in wt.%) from lowest (GWV-G-133B) to highest (FWV-G-34C).

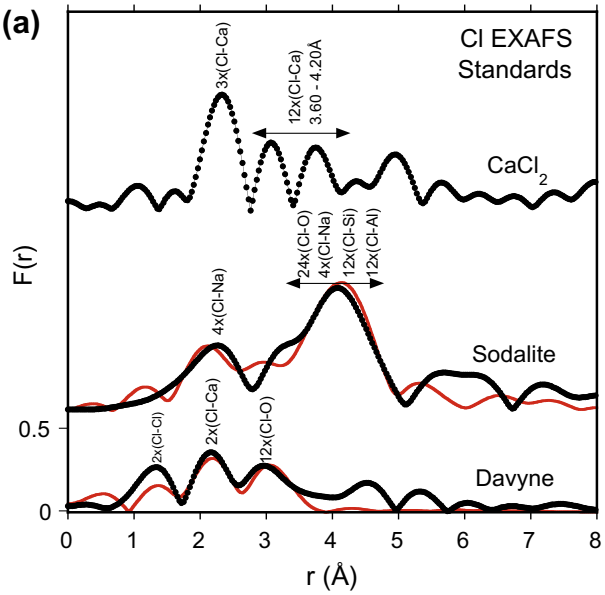

Fig. 5a. Partial RDFs of the standards, $CaCl_2$, sodalite, and davyne with pair correlations indicated for the major features. Final fits from FEFFIT (red lines) for sodalite and davyne are indicated. Plots are offset for clarity. (For interpretation of the references to colour in this figure legend, the reader is referred to the web version of this article.)

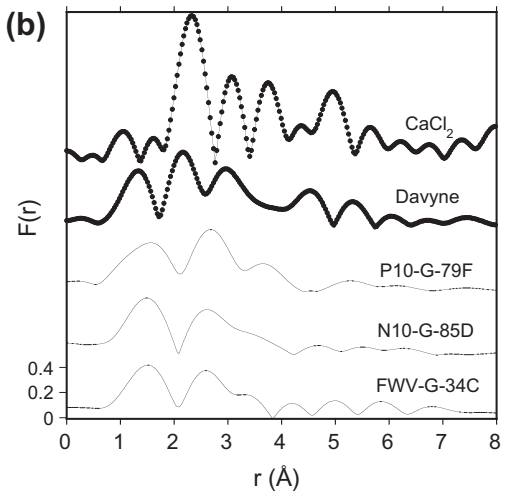

Fig. 5b. Partial RDFs of the $CaCl_2$ and davyne standards, as well as three representative glasses.

procedure, FEFFIT [22]. Atom clusters were generated to simulate the sodalite and davyne structures [11,12] that included atoms surrounding a central Cl out to a maximum radial distance of 5 Å. These clusters were used by FEFF7.02 [23] to calculate the theoretical EXAFS for each standard. The important atom pair correlations (or paths) calculated by FEFF for the atom clusters include Cl—Cl, Cl—Na, Cl—Ca, Cl—O, Cl—Si, and Cl—Al. These contributions could then be used to label the peaks in the partial RDFs for the standards (Fig. 5a), and were used in the fitting routines for sodalite, davyne, and the glasses. The position of each peak in the RDF is phase-shifted to lower r by approximately 0.5 Å with respect to the actual average bond distance that corresponds to each peak. For sodalite, the RDF fitting range was from 1.0 to 5.0 Å for the two nearest-neighbor peaks. Fitting for davyne used an RDF range from 0.25 to 4.0 Å for the first three nearest-neighbor peaks. Fitting for the three representative glasses included RDF features from 0.6 to 4.0 Å for the three overlapping nearest-neighbor peaks (Fig. 5b). At least two RDFs were fit for each sample.

EXAFS analyses of the $k^2\chi(k)$ data for sodalite and davyne determined s_0^2 and E_0 values that were used to fit features in the Cl partial RDFs for the glasses. The dominant contributions to the theoretical X-ray absorption spectrum for sodalite include the Cl—Na single scattering path at 2.74 Å [11] that is associated with the nearest-neighbor peak near 2.2 Å in the sodalite RDF (Fig. 5a middle); five other correlations describe the broad RDF peak near 4 Å that include twelve Cl—O at 4.29 Å, twelve Cl—O at 4.50 Å, four Cl—Na at 4.96 Å, as well as twelve Cl—Si and twelve Cl—Al at 4.97 Å. Due to the many pair correlations necessary to fit the major $k^2\chi(k)$ and RDF features for sodalite, it was necessary to constrain r, n, and σ^2 for each path to reasonably fit the data (Fig. 5a middle). Important paths from the davyne structure that describe most of the features in the $k^2\chi(k)$ and RDF data for davyne (Figs. 3a bottom and 5a bottom) include two Cl—Ca at 2.65 Å and twelve Cl—O at 3.75 Å [12]. The RDF peak centered near 1.3 Å cannot be described by the above two pair correlations because the shortest Cl—O and Cl—Ca distances in the two crystalline silicates studied are 3.41 and 2.67 Å, respectively. As a result, a short Cl—Cl distance path from the quadridavyne structure [16] was used in the fitting where the structural parameters were initially set to $r = 1.42$ Å and $n = 2.0$. Due to the nine fitting parameters used to describe the three major peaks in the RDF for davyne, n for the Cl—Ca and Cl—O paths were constrained to 2 and 12, respectively, to stably fit the data. E_0 and s_0^2 values of 3.1 eV and 0.80, respectively, were determined for the initial fits of the davyne data, where reasonable n and σ^2 values were used (Table 2). These E_0 and s_0^2 values were then held constant, while r, n, and σ^2 were varied to fit the nearest-neighbor peaks in the partial RDFs for the three representative glasses (Table 3 and Figs. 3b and 5b); these initial fits to the glass data led to unrealistically large n and σ^2 values, where fit oscillations were damped too strongly compared with the data. At this point, it was necessary to constrain σ^2 (Table 3), so that the fit better matched the higher k data (Fig. 6 bottom).

Table 2
Cl nearest-neighbor fitting results for davyne. The r-factor is a goodness of fit parameter that is a sum-of-squares measure of the fractional misfit scaled to the magnitude of the data [22]. Average values are listed with average uncertainties (in parentheses) calculated by FEFFIT. All fits used: $s_0^2 = 0.80$ and $E_0 = 3.1$ eV.

Standard	r-Factor	r (Å)	n (atoms)	σ^2 (Å^2)
Davyne	0.16			
Cl—Cl				
Fit		1.44 (0.09)	0.21 (0.04)	0.0055 (0.0163)
Cl—Ca				
Fit		2.67 (0.04)	2.0[a]	0.0187 (0.0096)
Actual [12]		2.65	2.0	
Cl—O				
Fit		3.73 (0.06)	12.0[a]	0.0418 (0.0156)
Actual [12]		3.75	12.0	

[a] Indicates constrained parameter.

4. Discussion

4.1. XANES

The Cl K-edge XANES spectra collected for the crystalline standards (Fig. 1) are similar to those shown earlier [2,4,24–27]. As Cl

Table 3
Chlorine nearest-neighbor fitting results for three representative glasses investigated, from low to high CaO content. Conventions in Table 2 used.

Glass	r-Factor	r (Å)	n (atoms)	σ^2 (Å^2)[a]
P10-G-79F				
Model 1	0.17			
Cl—Cl		2.45 (0.03)	7.1 (2.0)	0.0290
Cl—O		3.71 (0.04)	12.9 (2.0)	0.0180
Cl—Na		4.01 (0.04)	9.1 (1.8)	0.0095
Model 2	0.15			
Cl—Cl		2.44 (0.02)	7.6 (2.3)	0.0290
Cl—O		3.67 (0.04)	10.2 (1.8)	0.0180
Cl—O		4.09 (0.05)	7.6 (1.5)	0.0095
N10-G-85D				
Model 1	0.15			
Cl—Cl		2.44 (0.02)	8.2 (2.2)	0.0290
Cl—O		3.63 (0.05)	10.2 (1.5)	0.0180
Cl—Na		3.93 (0.06)	6.9 (1.3)	0.0095
Model 2	0.13			
Cl—Cl		2.43 (0.02)	8.0 (2.0)	0.0290
Cl—O		3.56 (0.05)	7.5 (1.5)	0.0180
Cl—O		3.96 (0.06)	5.7 (1.1)	0.0095
FWV-G-34C				
Model 1	0.17			
Cl—Cl		2.45 (0.04)	7.1 (2.8)	0.0290
Cl—O		3.55 (0.05)	10.7 (1.9)	0.0180
Cl—Na		3.85 (0.06)	8.2 (1.6)	0.0095
Model 2	0.12			
Cl—Cl		2.44 (0.02)	6.6 (1.9)	0.0290
Cl—O		3.52 (0.03)	7.8 (1.3)	0.0180
Cl—O		3.95 (0.04)	7.2 (1.4)	0.0095

[a] Indicates constrained parameter.

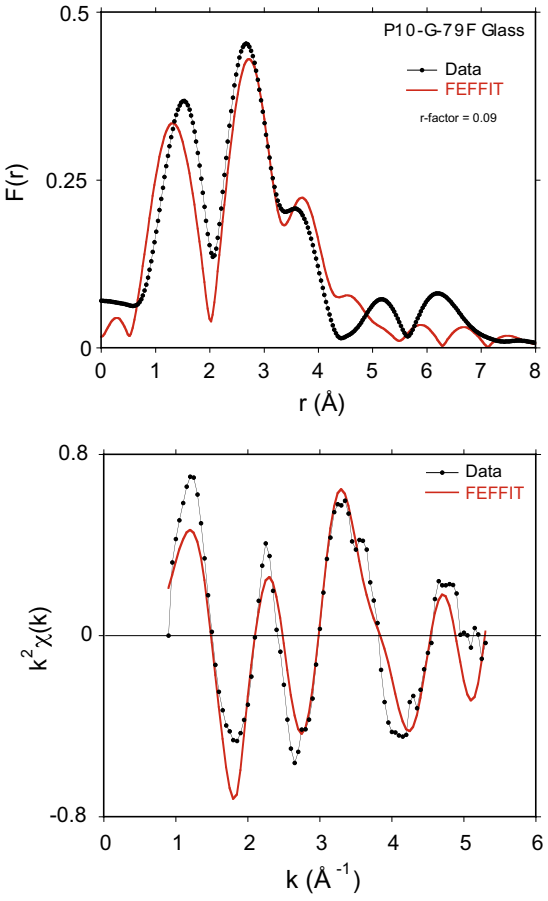

Fig. 6. EXAFS fitting results of the P10-G-79F $k^2\chi(k)$ and partial RDF data using the Cl—Cl, Cl—O, and Cl—Na model. Final fitting parameters are listed in Table 3 (Model 1).

becomes more reduced, the edges progressively shift to lower energies. Defining $E_0 = 2822.4$ eV, white line peaks are near 12.7 eV for Cl^{7+} within ClO_4 tetrahedra, and near 8.9 eV for Cl^{5+} within ClO_3 pyramids. More reduced Cl, such as Cl^{3+} in $NaClO_2$, and Cl^- in NaCl, KCl, and $CaCl_2$, have edge peaks near 4–5.5 eV. Both Cl—silicate standards, sodalite and davyne, have two edge maxima near 3.3 and 5.2 eV indicating reduced chlorine, or Cl^-, similar to that in NaCl, KCl, and $CaCl_2$. The edge peak is more pronounced in the sodalite XANES, where Cl is coordinated by Na, than in the davyne XANES where Cl is partially coordinated by Ca, and possibly, Cl.

XANES data for the glasses have two edge features near 3 and 6 eV (Fig. 2) that indicate reduced chlorine, or Cl^-, and are most similar to the Cl XANES of davyne, $CaCl_2$, and $CaCl_2{\cdot}2H_2O$ [2,4], where these materials have edge maxima near 2825 and 2827 eV (or near 3 and 5 eV using the energy scale in Fig. 2). $CaCl_2$, $CaCl_2{\cdot}2H_2O$, as well as davyne contain Cl^- bonded to Ca^{2+}. By comparing the glass data with the Cl XANES for crystalline standards measured here and elsewhere [2,4], Cl^- in these glasses is most likely coordinated with Ca.

The glass Cl edge features change most systematically with respect to CaO content out of all glass chemical components. By arranging the glass XANES data from lowest to highest CaO content (Fig. 2), which is generally from highest to lowest Na_2O content (Table 1), the edges progressively shift to slightly higher energies, where the high-energy edge shoulder (near 6 eV) becomes more pronounced. This trend roughly follows the XANES differences between davyne and $CaCl_2$ (Fig. 2). Cl XANES fitting was done in an earlier silicate glass study [2] using weighted mixtures of the NaCl and $CaCl_2{\cdot}2H_2O$ spectra, where the trends of the XANES mixtures were weighted more heavily toward $CaCl_2{\cdot}2H_2O$. Fitting the glass XANES spectra presented here could not be realistically done using the $CaCl_2$ data, due to the large amplitude of the edge features for this standard with respect to those for the glasses (Fig. 2). However, trends in the XANES indicate that as the glasses become more Ca-rich, the Cl environments evolve from probably a mixed-site type of structure like that in davyne to larger populations of sites that can be best described as disordered versions of the Cl-site in $CaCl_2$. The Cl^- environments in the glasses measured likely include multiple sites that have Ca nearest-neighbors, where Ca nearest-neighbors become more numerous as Ca is added to the glass.

4.2. EXAFS

4.2.1. Standards

The $k^2\chi(k)$ standards data (Fig. 3a) vary considerably with respect to each other, reflecting the considerably different atomic arrangements surrounding Cl in these phases. The data for the ClO_4, ClO_3, and ClO_2 standards have relatively large single frequency component oscillation amplitudes and periods that reflect contributions from simple environments around Cl, which contain oxygen atoms at Cl—O distances ranging from 1.46 to 1.57 Å (Fig. 3a top four plots). The $k^2\chi(k)$ data for NaCl and KCl have considerably shorter oscillation periods with smaller amplitudes (Fig. 3a middle two plots) that are due to surrounding Na and K cations with considerably longer distances from Cl (2.82 and 3.14 Å, respectively). The $k^2\chi(k)$ data for $CaCl_2$, sodalite, and davyne are each uniquely different with respect to the NaCl and KCl data, and show more complex oscillation amplitude behavior that suggests multiple contributing correlations at longer distances than those found in the Cl environments in the ClO_4, ClO_3, and ClO_2 standards (Fig. 3a bottom three plots). The $k^2\chi(k)$ data for $CaCl_2$, and especially davyne, more closely resemble the EXAFS for the glasses than any of the other standards (Figs. 3b and 4). The RDF for $CaCl_2$ is different with respect to those for davyne and the glasses (Fig. 5b top), where the relatively large amplitude 2.3 Å nearest-neighbor peak is due to one Cl—Ca distance at 2.70 Å and two Cl—Ca distances at 2.77 Å [10], while the series of features from 3.0 to 4.5 Å are due to twelve Cl—Cl correlations ranging from 3.60 to 4.20 Å. The RDF features for davyne are more similar to features in the glass RDFs than any of the other standards analyzed (Fig. 5b).

4.2.2. Glasses

EXAFS oscillations for the glasses are relatively weak and complex, and extend over a narrower k-space range compared with most standards (Figs. 3a, 3b, and 4). These differences indicate that several pair correlations contribute to the glass EXAFS data, similar to that for davyne. Due to the small amplitudes of these oscillations, the $k^2\chi(k)$ data have significant noise levels for some of the glass samples, especially at $k \geqslant 4$ Å^{-1}, even after averaging (Figs. 3b and 4). Like the XANES data, the glass EXAFS are most similar to that for $CaCl_2$, and especially davyne, that show trends dependent on CaO content in the glass (Fig. 4). As CaO concentration increases, the oscillation maximum near 1.2 Å^{-1} sharpens slightly, the oscillation maximum near 2.2 Å^{-1} broadens and shifts to 2.5 Å^{-1}, while oscillation amplitudes at higher k generally become smaller (Figs. 3b and 4). The RDFs for the glasses show significant differences, however, with respect to davyne, and especially $CaCl_2$ (Fig. 5b), and are dominated by two broad peaks near 1.6 and 2.7 Å that can be due to a variety of possible Cl correlations, when considering the nature of the Cl—silicate standards and glass compositions.

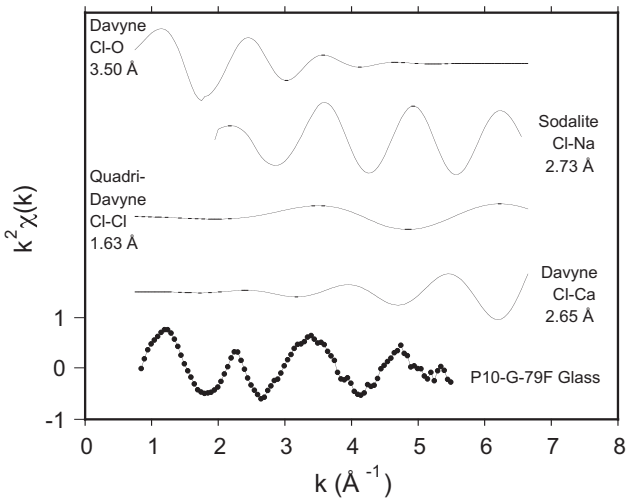

Fig. 7. FEFF calculated Cl—O, Cl—Na, Cl—Cl, and Cl—Ca $k^2\chi(k)$ contributions from the davyne and sodalite structures versus the $k^2\chi(k)$ data for a representative glass.

4.2.3. EXAFS fitting results

Due to the many fitting variables involved and nature of the EXAFS data, the fitting for the sodalite data was unstable when any parameters were varied. It was necessary to constrain all parameters, and then change each parameter by hand to obtain a reasonable fit to the data (Figs. 3a bottom and 5a middle). The final results used *r*- and *n*-values for the Na nearest-neighbors determined from the crystal structure refinement [11], as well as the Cl—O, Cl—Na, Cl—Si, and Cl—Al contributions to the broad 4 Å RDF peak (Fig. 5a middle), as outlined above; σ^2-values ranging from 0.0036 to 0.0066 Å^2 were used for the different paths.

The EXAFS fitting for davyne ran into similar stability problems, except that some structural parameters could be varied. The model that best fit the data used a Cl—Cl path for the RDF peak near 1.2 Å, Cl—Ca path for the RDF peak near 2.1 Å, and Cl—O path for the RDF peak near 3.0 Å (Fig. 5a bottom). The fitting used $E_0 = 3.5$ eV and $s_0^2 = 0.80$, while constraining Cl—Ca and Cl—O coordination numbers to values from the crystal structure refinement [12]; bond distance values refined to values near those determined for the crystal structure (Table 2). The coordination number for Cl—Cl was varied because of uncertainties for this site from the structure refinement; the small coordination number determined for the Cl—Cl correlation may be due to the site being partially occupied [12].

The analyses of the glass Cl EXAFS data were also difficult due to the narrow *k*-range and weak oscillation amplitudes. Different combinations of Cl—Cl, Cl—Na, Cl—Ca, and Cl—O correlations were initially tried to describe RDF features below 4 Å (Figs. 5b and 6). Due to the glass CaO-content relationship with features in the glass EXAFS data, Cl—Ca correlations were initially tried in the EXAFS fitting routines. However, any model using a Cl—Ca path failed to fit the data without varying *n* to negative values for that path. This behavior can be explained as follows: first, calculated Cl—Ca $k^2\chi(k)$ contributions have oscillations that are out-of-phase with respect to the glass data, and second, the most significant

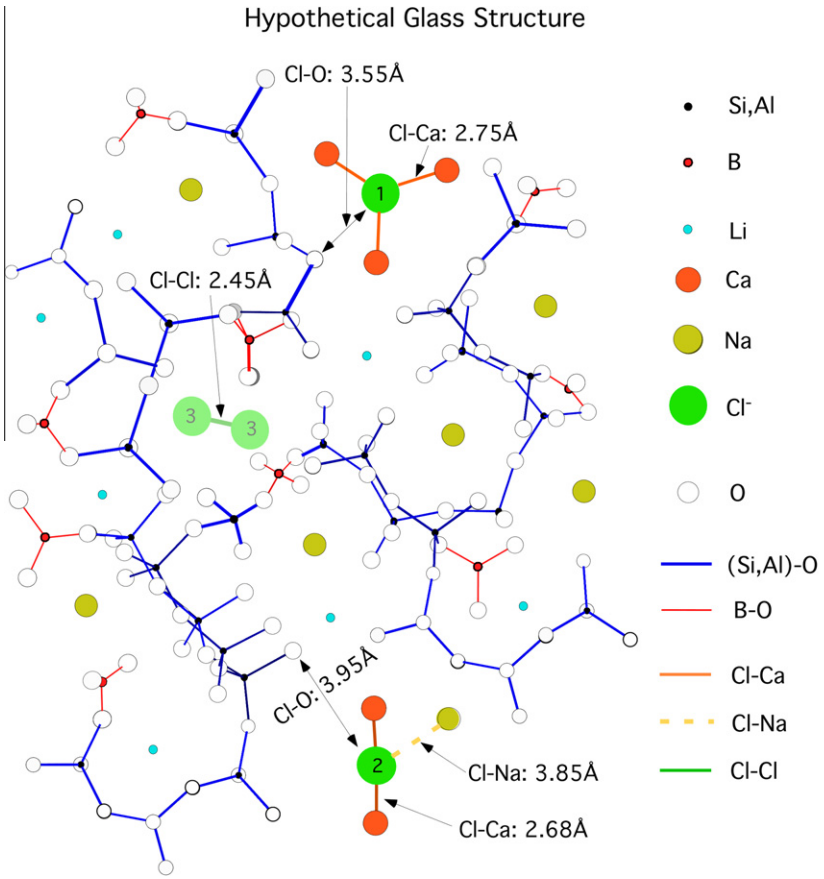

Fig. 8. Hypothetical FWV-G-34C glass structure depicting plausible Cl-sites determined from XAS. Numbers of atoms for each major element type shown approximate the glass composition. However, the four Cl atoms depicted are approximately ten times the true atomic proportion for Cl in this glass; the Cl atoms were included to show the different possible Cl-sites in the glass structure. Atomic distances from Cl are from EXAFS analysis, except for Ca—Cl, which are assigned from the XANES interpretations and are from the davyne and $CaCl_2$ structures. Most common Cl environments are site types 1 and 2; a possible Cl—Cl environment is site type 3 and would occur in small numbers (shown as partially transparent).

calculated Cl—Ca oscillation amplitudes are at $k > 5.0$ Å^{-1}, where the glass data essentially stop (Fig. 7). These trends are also seen in the $CaCl_2$ versus glass EXAFS data (Fig. 3b), where the Cl—Ca distances are slightly longer (~0.10 Å) than the davyne Cl—Ca path used in the fitting routines.

The model that best describes the glass EXAFS data used Cl—Cl and two Cl—O correlations to fit the three RDF peaks (Fig. 6), where Debye–Waller factors were constrained to large values, due to the narrow k-range of the data; as a result, n-values determined from the fitting were large (Table 3). Another model that reasonably fit the data used Cl—Cl, Cl—O, and Cl—Na correlations (Table 3); calculated contributions for the davyne Cl—O and sodalite Cl—Na paths can describe most of the features in the $k^2\chi(k)$ glass data (Fig. 7). The useful values determined from the fitting are the distance parameters only; the three sets of n and σ^2 from these fits cannot be considered meaningful, because these six variables are heavily correlated with each other and are strongly influenced by the narrow k-range of EXAFS oscillations for the glasses. Overall, Cl—O and Cl—Na distances decrease by 0.16 Å as CaO content increases (Table 3). These distance changes are due to the EXAFS oscillation period becoming longer as the glasses become more Ca-rich (Figs. 3b and 4). These models may not be the only explanations of the Cl EXAFS features for the borosilicate glasses investigated, but are the best we can obtain, considering the nature of the data and the Cl—silicate crystal structures used as standards.

The narrow k-space EXAFS ranges for the glasses may be due to interfering pair correlations from the glass structure, that damp EXAFS amplitude at larger k values. Cl—Na and Cl—Ca paths used in the theoretical models to fit the glass EXAFS data are out-of-phase with respect to each other (Fig. 7). If these contributions exist in the glass structure surrounding Cl, then any EXAFS amplitude would be significantly damped starting at $k = 5$ or 6 Å^{-1}. This can explain why the glasses have no appreciable EXAFS amplitude beyond 6 Å^{-1} (Figs. 3b and 4).

4.3. Glass structural models

Two lines of XAS evidence indicate that Cl has an affinity for Ca in the borosilicate glasses investigated, especially as Ca concentrations in glass become larger. Cl^- in these glasses is likely to be in multiple sites that have Ca nearest-neighbors; second- and third-nearest neighbors in these sites are likely to include oxygen atoms from the surrounding tetrahedral network, and possibly Na. From the XANES evidence, the majority of Cl atoms in these glasses have Ca nearest-neighbors, where these environments can be of two main types: one, a disordered version of the Cl-site in $CaCl_2$ (Fig. 8, site 1), with three coordinating Ca atoms at different Cl—Ca distances that average near 2.75 Å; and two, a disordered version of the Ca—Cl—Ca site in davyne (Fig. 8, site 2), with two different Cl—Ca distances that average around 2.68 Å. Unfortunately, Cl—Ca distances and number of Ca nearest-neighbors around Cl in these sites could not be quantitatively determined from the EXAFS data. However, according to EXAFS, the average environment surrounding Cl has three other possible pair correlations: Cl—Cl distances near 2.45 Å (Fig. 8, site 3) that do not appreciably change with respect to glass composition, and two longer distance Cl—O (or possibly, Cl—O and Cl—Na) correlations between 3.5 and 4.0 Å that decrease by 0.16 Å as Ca concentrations increase in the glass (Table 3).

The EXAFS results for the longer distance changes around Cl may be related to how the polymerized tetrahedral networks in the silicate glass structure respond to Ca^{2+} replacing Na^+ in the network modifying sites. Feldspar structures have been used to model silicate glasses; features from these crystal structures may provide guidelines to view how the glass structure may adjust when alkali and alkaline earth cations are changed. Average alkali and alkaline earth cation to oxygen distances in feldspar structures include Na—O at 2.81 Å in albite ($NaAlSi_3O_8$) [28], and Ca—O from 2.49 to 2.55 Å in anorthite ($CaAl_2Si_2O_8$) [29]. The shorter distances around Ca^{2+} versus Na^+ in aluminosilicate crystals suggest smaller distances across network voids in a glass as Na^+ is replaced by Ca^{2+}. Looking at the tetrahedral network within a glass structure, the term "ring statistics" or ring size distribution is often used, which is the distribution of n-membered rings that make up the network, where n is the number of linked SiO_4 or AlO_4 tetrahedra within that ring. Arguments have been made for feldspar composition glasses, where tetrahedral networks change ring statistics when Na^+ is replaced by Ca^{2+} [30], while more Al tetrahedra are incorporated into the network for charge balance. By using X-ray radial distribution analysis [30], albite glass was found to have tridymite-like networks consisting primarily of 6-membered rings (larger network voids), while anorthite glass networks consist of 4- and 6-membered rings (smaller network voids). These ring size distribution differences should also affect Cl environments that are probably within similar voids and may be the cause behind the second- and third-nearest neighbor distance changes around Cl in relation to the CaO/Na_2O content of the glass.

The XAS evidence for the glasses indicate that Cl may be in at least three sites. Two types of sites have isolated Cl^- with Ca^{2+} nearest-neighbors (Fig. 8, sites 1 and 2). Site 2 would be more common in the Ca-poor glasses. As the glasses become more Ca-rich, site type 2 populations may decrease, while site type 1 populations would increase. In many of these sites, Cl probably has oxygen second-nearest neighbors as well as oxygen or Na third nearest-neighbors (Fig. 8). The evidence for Cl—Cl bonding is the weakest out of all Cl environmental details determined from XAS in this study. However, for completeness, we conclude that Cl—Cl sites may exist (Fig. 8, site 3) as a small fraction of all Cl-sites in borosilicate glass structure.

5. Conclusions

Chlorine XAS data were collected for 15 borosilicate glasses, where the XANES and EXAFS data both vary systematically with respect to CaO concentration. XANES trends for the Ca-poor glasses indicate multiple Cl^- environments that may be similar to those in davyne (mostly with two Ca nearest-neighbors), while in the more Ca-rich glasses, larger Cl-site populations may be disordered versions of the Cl-site in $CaCl_2$ (three Ca nearest-neighbors). Cl EXAFS data analyses indicate at least three possible contributions: Cl—Cl near 2.45 Å, Cl—O near 3.60 Å, and Cl—O (or Cl—Na) near 3.90 Å. As Ca replaces Na in these glasses, Cl—O, and possibly Cl—Na, distances decrease, which may be due to smaller voids within the glass network as a structural adjustment. Findings from EXAFS theory also indicate that any Cl—Ca contributions to the glass EXAFS probably interfere with other pair correlations to damp EXAFS oscillations so that there is little to no signal beyond $k = 5.0$ Å^{-1}; this would virtually eliminate any discernable Cl—Ca contributions in the EXAFS data for the glasses investigated, even though Cl probably has Ca nearest-neighbors in most Cl-sites. EXAFS analyses suggest the possibility of small populations of Cl—Cl sites in the borosilicate glass structure. Overall, XAS data and analysis results presented here for Cl are generally consistent with earlier findings from XANES and NMR studies of Cl in silicate glasses that describe Cl being in network modifying sites with Na^+ and Ca^{2+} nearby.

Acknowledgments

We thank J.E. Post and P. Pohwat (Mineral Sciences Department, National Museum of Natural History, Smithsonian Institution) for

supplying the standards: halite, sylvite, davyne, and sodalite. Preparation of some of the samples used in this work was supported in part by the U.S. Department of Energy (DOE) Office of River Protection through *Energy Solutions*, Inc. The Advanced Light Source is supported by DOE (DE-AC03-76SF00098).

References

[1] Keith Matlack, Isabelle Muller, Weiliang Gong, Ian L. Pegg, Small Scale Melter Testing of LAW Salt Phase Separation, Final Report VSL-07R7480-1 Rev. 0, Vitreous State Laboratory, The Catholic University of America Washington, DC, 2006.
[2] K.A. Evans, J.A. Mavrogenes, H.S. O'Neill, N.S. Keller, L.-Y. Jang, Geochem. Geophys. Geosystems 9 (2008) Q10,003.
[3] T.O. Sandland, L.-S. Du, J.F. Stebbins, J.D. Webster, Geochim. Cosmochim. Acta 68 (2004) 5059–5069.
[4] F. Zhu, Technological Development of an Effective Recycling System for Fly Ash from Municipal Solid Waste Incinerator to be Raw Material in the Cement Industry, Ph.D. Thesis, Chptr 3., Dept. Urban and Environmental Engineering, Kyoto University, Kyoto, Japan, 2008.
[5] R.G.W. Wyckoff, Crystal Structures, vol. 3, John Wiley & Sons, New York, 1965, p. 19.
[6] R.G.W. Wyckoff, Crystal Structures, vol. 3, 1965 p.48.
[7] R.G.W. Wyckoff, Crystal Structures, vol. 2, 1965 p.380.
[8] C. Tarimici, R.D. Rosenstein, E. Schempp, Acta Cryst. B32 (1976) 610–612.
[9] D. Walker, P.K. Verma, L.M.D. Cranswick, R.L. Jones, S.M. Clark, S. Buhre, Am. Min. 89 (2004) 204–210.
[10] R.G.W. Wyckoff, Crystal Structures, vol. 1, 1963 p.252.
[11] I. Hassan, S.M. Antao, J.B. Parisse, Am. Min. 89 (2004) 259–264.
[12] I. Hassan, H.D. Grundy, Can. Min. 28 (1990) 341–349.
[13] K.S. Matlack, H. Hojaji, S.S. Fu, I.L. Pegg, P.B. Macedo, Ceram. Trans. 61 (1995) 221.
[14] S.S. Fu, W. Luo, H. Hojaji, M. Brandys, R.K. Mohr, K.S. Matlack, I.L. Pegg, P.B. Macedo, Ceram. Trans. 72 (1996) 27.
[15] W. Brendler, Am. Mineral. 19 (1934) 28–29.
[16] E. Bonaccorsi, S. Merlino, P. Orlandi, M. Pasero, G. Vezzalini, European. J. Min. 6 (1994) 481–487.
[17] D. Haskel, The Executable Code and Documentation, 1999. <www.aps.anl.gov/xfd/people/haskel/fluo.html>.
[18] C.H. Booth, F. Bridges, Phys. Scr. T 115 (2005) 202–204.
[19] R.C.C. Perara, P.L. Cowan, D.W. Lindle, R.E. LaVilla, T. Jach, R.D. Deslattes, Phys. Rev. A 43 (1991) 3609–3618.
[20] R. Guillemin, S. Carniato, W.C. Stolte, L. Journel, R. Taieb, D.W. Lindle, M. Simon, Phys. Rev. Lett. 101 (2008) 133003–133007.
[21] D.E. Sayers, B.A. Bunker, in: D.C. Kroningsberger, R. Prins (Eds.), X-ray Absorption Principles, Applications, Techniques of EXAFS, SEXAFS, and XANES, Wiley, New York, 1988, p. 211. Chapter 6.
[22] M. Newville, B. Ravel, D. Haskel, E.A. Stern, Y. Yacoby, Physica B 208–209 (1995) 154–156.
[23] S.I. Zabinsky, J.J. Rehr, A. Ankudinov, R.C. Albers, M.J. Eller, Phys. Rev. Lett. B 52 (1995) 2995–3009.
[24] S.E. Shadle, B. Hedman, K.O. Hodgson, E.I. Solomon, Inorg. Chem. 33 (1994) 4235–4244.
[25] A. Filipponi, T.A. Tyson, K.O. Hodgson, S. Mobillo, Phys. Rev. A 48 (1993) 1328–1333.
[26] M. Kigachi, T. Yokoyama, D. Matsumura, H. Kondoh, T. Ohta, Y. Kitajima, Phys. Rev. B 60 (1999) 16205–16210.
[27] V. Gotte, J. Goulon, C. Goulon-Ginet, A. Rogalev, C.R. Natoli, K. Perie, J.-M. Barbe, R. Guilard, J. Chem. Phys. B 104 (2000) 1927–1938.
[28] J.K. Winter, F.P. Okamura, S. Ghose, Am. Min. 64 (1979) 409–423.
[29] R.J. Angel, Am. Min. 73 (1988) 1114–1119.
[30] M. Taylor, G.E. Brown Jr., Geochim. Cosmochim. Acta 43 (1979) 61–75.